

Thin Films of Molybdenum Disulfide Doped with Chromium by Aerosol-Assisted Chemical Vapor Deposition (AACVD)

David J. Lewis,^{†,‡,§} Aleksander A. Tedstone,^{†,§} Xiang Li Zhong,[‡] Edward A. Lewis,[‡] Aidan Rooney,[‡] Nicky Savjani,[§] Jack R. Brent,[‡] Sarah J. Haigh,[‡] M. Grace Burke,[‡] Christopher A. Muryn,[§] James M. Raftery,[§] Chris Warrens,^{||} Kevin West,^{||} Sander Gaemers,[⊥] and Paul O'Brien*,^{†,‡,§}

[†]International Centre for Advanced Materials (ICAM), University of Manchester, Manchester M13 9PL, United Kingdom

[‡]School of Materials, University of Manchester, Oxford Road, Manchester M13 9PL, United Kingdom

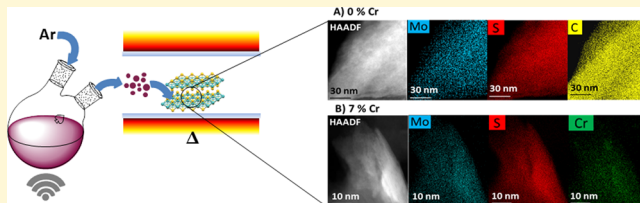
[§]School of Chemistry, University of Manchester, Oxford Road, Manchester M13 9PL, United Kingdom

^{||}BP Technology Centre, Whitchurch Hill, Pangbourne, Berkshire RG8 7QR, United Kingdom

[⊥]Castrol innoVentures, BP Technology Centre, Whitchurch Hill, Pangbourne, Berkshire RG8 7QR, United Kingdom

Supporting Information

ABSTRACT: A combined single-source precursor approach has been developed for the deposition of thin films of Cr-doped molybdenum disulfide (MoS_2) by aerosol-assisted chemical vapor deposition (AACVD). Tris-(diethyldithiocarbamato)chromium(III) can also be used for the deposition of chromium sulfide (CrS). Films have been analyzed by a range of techniques including scanning electron microscopy (SEM), energy dispersive X-ray (EDX) spectroscopy, Raman spectroscopy, and powder X-ray diffraction (pXRD) to elucidate film morphology, composition, and crystallinity. The presence of Cr in the MoS_2 films produces a number of striking morphological, crystallographic, and nanomechanical changes to the deposited films. The chromium dopant appears to be uniform throughout the MoS_2 from the scanning transmission electron microscopy (STEM) EDX spectrum imaging of nanosheets produced by liquid-phase exfoliation of the thin films in *N*-methyl-2-pyrollidone.



INTRODUCTION

The synthesis of molybdenum disulfide (MoS_2) as semiconducting thin films,¹ nanoparticles,^{2–5} or as two-dimensional graphene analogues^{6–11} has attracted considerable attention. MoS_2 has also attracted interest for catalytic applications including hydrodesulfurisation of petroleum¹² and hydrogen generation.^{13,14} Prior to the relatively recent use of MoS_2 for high-tech applications, it has been used for almost 40 years in the automotive industry as a solid lubricant to reduce both friction and thus wear in engines.¹⁵ The transition metal dichalcogenide, tungsten disulfide (WS_2), is also often used as a lubricant. In the case of motor oils these materials are, on the whole, introduced via a dispersible precursor molecule, typically dialkyldithiocarbamato molybdenum (MoDTC) species with the MoS_2 being formed *in situ* under the relatively high conditions of temperature and pressure found in engine systems. In lubricating greases, the additives are often introduced directly as solid MoS_2 or WS_2 because sedimentation in these matrices is not an issue.¹⁶

The ability of MoS_2 to act as an effective lubricant arises primarily from its layered structure (Figure 1). The unit cell of MoS_2 contains two layers of molybdenum and sulfur ions bound together.¹⁷ Various polytypes are possible with 2H- MoS_2 being the most common.¹⁸ In the layers, molybdenum ions are hexagonally close-packed with trigonal prismatic

coordination at sulfur. The distinct S–Mo–S layers are held together by weak noncovalent interactions often described as van der Waals forces. Hence, under lateral stress, MoS_2 is prone to intracrystalline shear between its layers, and thus the material acts as a lubricant.^{16,19} Reflecting this, the coefficient of friction, defined as the dimensionless scalar between applied force normal to a surface and the force required to move an object laterally, is typically found to be 0.1 or lower for MoS_2 -coated surfaces against a sliding steel counterpart. The coefficient of friction of steel sliding on steel is around 0.8, whereas that of a Teflon-coated surface against a sliding steel counterpart is around 0.05. These values refer to unlubricated contact, and under lubricated conditions, the coefficient of friction can be significantly lower. MoS_2 is very useful in extreme conditions as it, unlike the majority of lubricants, maintains its performance in vacuum.²⁰ However, even though MoS_2 displays good lubricity, it is not necessarily hard (Vickers Hardness,²¹ $H_v \sim 500$) and therefore perhaps not persistent with regard to its resistance to plastic deformation. The elastic modulus (E) of lubricant transfer films is also crucial to their tribological performance in applications, with respect to elastic deformation

Received: December 10, 2014

Revised: January 30, 2015

Published: January 31, 2015

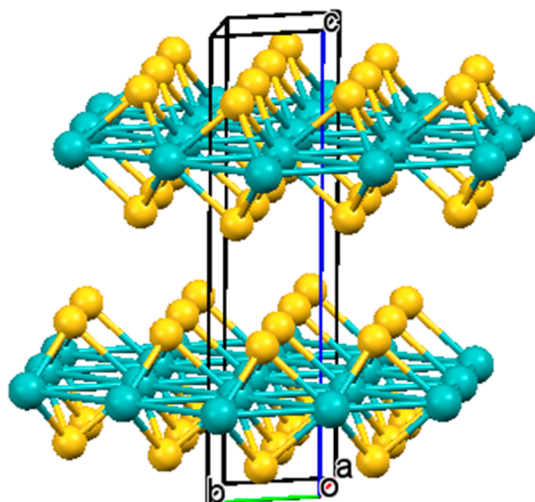


Figure 1. Layer structure of 2-H MoS₂ after Pauling and co-workers.¹⁷ Sulfur ions are represented by yellow spheres, molybdenum ions are represented by blue spheres. The unit cell is marked with $a = 3.15(2)$ Å $b = 3.15(2)$ Å $c = 12.30(7)$ Å and $\alpha = 90^\circ$ $\beta = 90^\circ$, $\gamma = 120^\circ$. Space group P6₃/mmc.

of transfer films.¹⁶ Shtanskiĭ et al. have suggested that the resistance to deformation of a material under sliding contact can be described using the parameter H^3/E^2 .²² In engines, the material is essentially sacrificial and needs to be replenished by having a constant supply of the molecular precursors (dialkylthiocarbamatomolybdenum complexes) as an additive in the engine oil. There are increasingly stringent limits on the amount of phosphorus and sulfur allowed in engine oils; in 2009, the international lubricant standardization and approval committee's (ILSAC) GF-5 limits were defined as 0.06 wt % $\leq P \leq 0.08$ wt % for total phosphorus (ASTM 4951) and similarly, 0.50 wt % $\leq S$, for total sulfur contained in the oil (ASTM 4951 or 2622). The limits have been introduced as guidelines by engine manufacturers primarily for protection of vehicle exhaust after-treatment systems, due to the potential for poisoning of catalytic converters, with sulfated ash restrictions applied to vehicles equipped with exhaust particulate filter systems. Any chemical modification able to increase the durability of MoS₂ is highly sought-after as it can improve the tribological properties of the MoS₂ produced *in situ* and less of its molecular precursor are needed in the oil.

We have been interested in the deposition of metal chalcogenide materials such as MoS₂ by techniques such as aerosol-assisted chemical vapor deposition (AACVD)^{23,24} using single-source inorganic precursors (SSPs).¹ The advantages of using precursors to produce metal chalcogenide thin films has been outlined.²⁵ In brief, it allows control of molecular stoichiometry, avoidance of prereaction and generally leads to purer thin films due to the preorganization of bonds. In the production of sulfides in particular, it avoids the use of hydrogen sulfide with its associated toxicity hazards. There is precedent for the doping of films with transition metal elements such as titanium using a dual precursor approach and AACVD,²⁶ although there were negligible improvements in lubrication performance upon titanium doping. However, Stupp and co-workers have reported that chromium-doped MoS₂ has stable frictional properties and improved durability.²⁷ Ding et al. reported the doping of MoS₂ with chromium and titanium by using unbalanced magnetron sputtering and found

that the hardness of the films produced were increased compared with the parent MoS₂.²⁸ Similarly, Kao et al. have reported the use of chromium to dope MoS₂ using magnetron sputtering to produce an optimum coating for wear testing with bearings made of copper, steel as well as ceramic materials—the latter perhaps representing an important anticipatory result for the identification of potential lubricants which perform well with nonferrous materials.²⁹ Surfaces coated with molybdenum sulfide films alloyed with Al and Ti produced by Fenker et al. were reported to have improved resistance versus corrosion in salt spray tests compared to MoS₂.³⁰ Simmonds et al. produced films of MoS₂ containing Au, Ti, Cr or another metal dichalcogenide, such as WSe₂, by magnetron cosputtering for a variety of standard wear tests; doped films were observed to indeed be more persistent compared with the parent compound.³¹ However, despite the large body of work toward improving the properties of MoS₂, the coating processes generally used are unsuitable for scale-up as they require the use of high vacuum plasma techniques. With regard to doping of MoS₂ for optoelectronic applications, a method was very recently described to substitutionally cation-dope MoS₂ with niobium to produce a *p*-type semiconductor (i.e., against the natural propensity of MoS₂ for *n*-type semiconduction) by chemical vapor transport (CVT) using iodine as a transport agent, but which required vacuum in excess of 10^{-6} Torr. Hence, a facile procedure to deposit Cr-doped MoS₂ which may have improved tribological properties compared with MoS₂, as well as tunable semiconductivity is highly attractive for instance in the coating of engine components prior to their assembly and in semiconductor research; AACVD provides a simple method to rapidly deposit thin films of the doped metal chalcogenides which does not require high vacuum. Furthermore, exfoliation of materials, produced by AACVD, in solvents such as *N*-methyl-2-pyrrolidone could provide a potential route to doped nanosheets which may have optoelectronic properties differing from the parent compound for applications such as inkjet printing of novel two-dimensional semiconductors.^{32,33}

In this paper, we outline the deposition of Cr-doped MoS₂ films by a dual-precursor approach using aerosol-assisted chemical vapor deposition (AACVD) to deposit films on glass, and we report the properties of the doped films versus films comprised of MoS₂. A route to chromium(II) sulfide (CrS) thin films from a single source precursor is also reported.

EXPERIMENTAL SECTION

General. All manipulations were carried out under a dry nitrogen atmosphere using standard Schlenk techniques. Solvents were purchased from Sigma-Aldrich or Fisher and used without further purification. Reagents were purchased from Sigma-Aldrich.

Instrumentation. ¹H NMR spectroscopy was performed using a Bruker AVIII400 NMR spectrometer. Electrospray mass spectra were recorded using a Micromass Platform II instrument. Melting points were carried out using a Stuart SMP-10 digital melting point apparatus. FT Infrared absorption spectra were recorded using a Thermo Scientific iDS-ATR spectrometer. Microanalysis was performed using a Thermo Scientific Flash 2000 Organic Elemental Analyzer. Thermogravimetric analyses were performed using Mettler-Toledo TGA/DSC 1. Scanning electron microscopy (SEM) was performed in secondary electron mode with a Zeiss Ultra55 microscope with an accelerating voltage of 2–3 kV. Energy-dispersive X-ray (EDX) spectroscopy was performed on the same system at an accelerating voltage of 30 kV using an Oxford Instruments INCA pentaFETx3 detector. Samples for SEM imaging were mounted on stubs using conductive Leit carbon tabs (Agar Scientific). Raman spectroscopy was performed using a Renishaw 1000 microscope system equipped with a 50 × objective,

with solid-state laser excitation (514.5 nm, 20% power). The incident light was linearly polarized in the sample plane with scattered light left unanalyzed for collection by the air cooled CCD. Bright-field images were collected using a standard CCD camera. Powder X-ray diffraction (pXRD) measurements were made using a Bruker D8 Discover diffractometer using Cu K α radiation (1.54178 Å). Single crystal X-ray diffraction experiments were run using a Bruker Prospector diffractometer using Cu K α radiation (1.546 Å). The structure was solved by direct methods and refined by full-matrix least-squares fit on F². All non-H atoms were refined anisotropically. All calculations were carried out using SHELXTL.³⁴ Atomic force microscopy (AFM) was performed using a Bruker Multimode 8 AFM in equipped with a silicon nitride tip in PeakForce QNM mode. Transmission electron microscopy (TEM) imaging was performed using a FEI Tecnai T20 TEM operated at 200 kV. High-angle annular-dark-field (HAADF) STEM imaging and EDX spectrum imaging were performed using a probe side aberration corrected FEI Titan G2 80–200 S/TEM “ChemiSTEM” instrument operated at 200 kV, with a convergence angle of 18.5 mrad, a HAADF inner angle of 54 mrad and a probe current of ~200 pA. EDX spectra and spectrum images were analyzed using Bruker Esprit software and HAADF STEM images were analyzed using Gatan Digital Micrograph Software.

Tetrakis(diethyldithiocarbamato)molybdenum(IV) (MoL_4). MoL_4 was produced using the method of Decoster et al.³⁵ Briefly, molybdenum hexacarbonyl (1.0 g, 3.7 mmol, 1.0 equiv) was heated to reflux in acetone (40 mL) in the presence of tetraethylthiuram disulfide (2.3 g, 7.4 mmol, 2.0 equiv), and the mixture was held for 2 h at this temperature. The reaction mixture was then allowed to cool slowly over an hour to room temperature, affording the crystallization of a black microcrystalline solid, which was isolated by suction filtration and washed with pentane (3 × 20 mL) to afford the title product (1.5 g, 59%); mp 119–124 °C (dec.). ES-TOF⁺ *m/z*: 689 {M + H}⁺. FT-IR (solid) $\nu_{\text{max}}/\text{cm}^{-1}$: 2970 (w), 2930 (w), 2869 (w), 1517 (m), 1490 (m), 1454 (m), 1427 (m), 1374 (m), 1352 (m), 1269 (m), 1211 (m), 1145 (m), 1094 (m), 1074 (m), 1001 (m). Anal. Calcd for $\text{C}_{20}\text{H}_{40}\text{N}_4\text{S}_8\text{Mo}$: C, 34.9; H, 5.9; N, 8.1. Found: C, 34.9; H, 6.2; N, 8.0%.

Tris(diethyldithiocarbamato)chromium(III) (CrL_3). To a green solution of chromium trichloride hexahydrate (4.0 g, 18 mmol, 1.0 equiv) in water (250 mL) adjusted to pH 5 by the addition of concentrated hydrochloric acid was added the monosodium salt of diethyl dithiocarbamate (12.0 g, 54 mmol, 3.0 equiv) in portions which effected a color change to blue. Precipitation of a blue solid rapidly followed, which was removed by filtration to afford crude CrL_3 . The chromium complex was purified using column chromatography on silica eluting dichloromethane or chloroform, collecting the rapidly eluted brilliant blue band. The solvent was removed under vacuum to afford CrL_3 as an ultramarine solid (1.2 g, 13%); mp 260–261 °C (dec.). ¹H NMR (400 MHz, CDCl_3 , δ/ppm : 23.9 (s, CH_2), 12.5 (s, CH_2), 0.5 (s, CH_3). ES-TOF⁺ *m/z*: 519 {M + Na}⁺, 497 {M + H}⁺. FT-IR (solid) $\nu_{\text{max}}/\text{cm}^{-1}$: 2972 (w), 2930 (w), 2868 (w), 1490 (m), 1460 (m), 1450 (m), 1434 (m), 1376 (m), 1357 (m), 1268 (m), 1207 (m), 1141 (m), 1098 (m), 1075 (m), 995 (m). Anal. Calcd for $\text{C}_{15}\text{H}_{30}\text{N}_3\text{S}_6\text{Cr}$: C, 36.3; H, 6.1; N, 8.5%. Found: C, 37.0; H, 6.6; N, 8.3. Single crystals suitable for single crystal X-ray diffraction experiments were grown from vapor diffusion of hexane into a chloroform solution (approximately 10 mg mL⁻¹ CrL_3) of the purified complex.

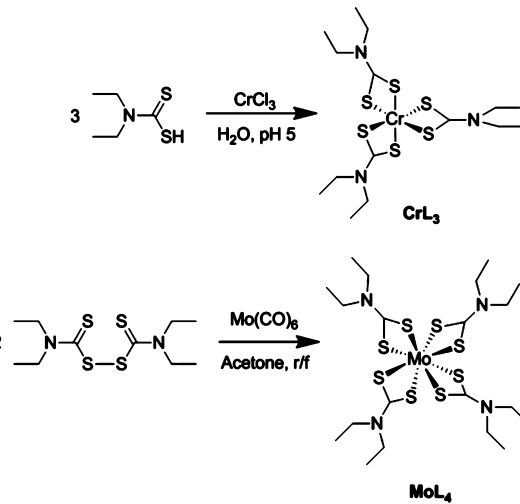
Aerosol-Assisted Chemical Vapor Deposition (AACVD). The apparatus has been described in detail previously.^{36,37} In a typical experiment, 0.29 mmol of total precursors (i.e., mol MoL_4 + mol CrL_3) were dissolved in tetrahydrofuran (25 mL) to give solutions with varying mole ratios of MoL_4 and CrL_3 . The solution was held over a piezoelectric humidifier and the aerosol thus created was carried by a stream of argon (flow rate: 160–180 cm³ min⁻¹) into a quartz tube containing eight glass substrates of dimensions ca. 3 cm × 1 cm laid out end-to-end. The tube was housed in a Carbolite furnace set to either 450 or 500 °C. The deposition of metal chalcogenides onto glass substrates was continued for 100 min in all cases.

Liquid-Phase Exfoliation of MoS_2 . The setup for exfoliation has been described in detail previously.³⁸ Briefly, MoS_2 films on glass substrates produced from AACVD were ultrasonicated in *N*-methyl-2-pyrrolidone for 48 h using an Elmasonic P 70H benchtop ultrasonic bath (820 W across four horns) operating at 37 kHz frequency and 30% power. The bath was modified by the addition of a water-cooling coil to maintain the bath temperature below 30 °C during sonication. The resulting solutions were drop cast onto holey carbon grids for analysis using HAADF STEM and EDX spectroscopy imaging.

■ RESULTS AND DISCUSSION

The synthesis of molecular precursors CrL_3 and MoL_4 was carried out according to Scheme 1. CrL_3 was produced by

Scheme 1



simple direct reaction of the ligand and chromium(III) chloride, whereas MoL_4 was produced by oxidative addition of tetraethyl dithiuram to molybdenum(0) hexacarbonyl according to the method of Decoster et al.³⁵ The yield of the former reaction was markedly low due to the difficulty in preparing (*N,N*-dithiocarbamato)chromium(III) complexes.³⁹ Elemental analysis, infrared spectroscopy, and mass spectrometry confirmed the purity of the complexes. ¹H NMR of CrL_3 matched well with that reported by Golding et al.³⁹

Single crystals of CrL_3 suitable for X-ray diffraction experiments were grown by the diffusion of hexane into a chloroform solution of CrL_3 . The structure produced is a slightly distorted octahedral complex, with three dithiocarbamate ligands coordinated to the Cr(III) center in a bidentate fashion as expected with sulfur atoms coordinated equidistantly to chromium by a distance of ca. 2.40 Å (Supporting Information), mirroring the crystal structure previously presented by Raston et al.; however, in our case, CrL_3 crystallized in the monoclinic *p2(1)/n* space group.⁴⁰

Thin films of MoS_2 , chromium-doped MoS_2 , or CrS were grown by AACVD. A THF solution of either MoL_4 or CrL_3 for pure MoS_2 or CrS , respectively, or a mixture containing both precursors for Cr-doped MoS_2 films (MoL_4 containing 10 mol %, 20 mol %, 30 mol %, 50 mol % CrL_3) was nebulized, and the vapor, carried by a stream of argon gas, was thermally decomposed on the substrate. Thermogravimetric analysis (TGA) was used to target a temperature range in which decomposition of both precursors occurs simultaneously. CrL_3 displayed a one-step profile with an inflection at 385 °C with overall 89% weight loss, corresponding to decomposition to

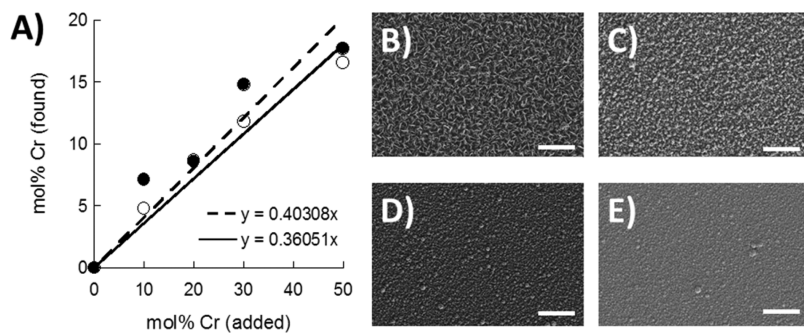


Figure 2. EDX spectroscopy of MoS₂ thin films doped with varying amounts of chromium. (A) Comparison of theoretical amount of chromium doped into MoS₂ films and the amount found experimentally by using EDX spectroscopy for deposition at 450 °C (● and - - - linear fit) and 500 °C (○ and — linear fit). Secondary electron SEM images: (B) 0% Cr (MoS₂), (C) 7.1% Cr, (D) 8.4 mol % Cr, (E) CrS; prepared at 450° by AACVD. All scale bars represent 5 μm.

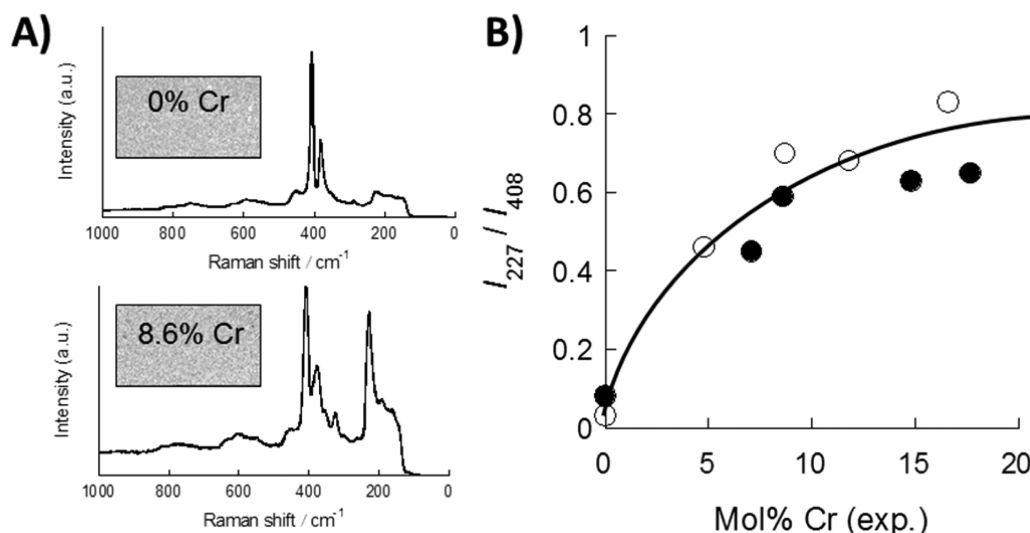


Figure 3. (A) Raman spectra of 0% and 8.6% Cr-doped MoS₂ thin films deposited at 450 °C. Insets: bright-field reflectance images of thin films at 50× magnification. (B) Plot of integrated peak intensity ratio at 227 and 408 cm⁻¹ vs chromium dopant found experimentally by using EDX spectroscopy for deposition at 450 °C (●) and 500 °C (○). Line is provided as a trend guide and is not a fitted function.

CrS (Supporting Information), whereas **MoL₄** displayed a four-step degradation profile as observed previously for this precursor.²⁶ Hence, two temperatures were selected to produce the double-decomposition required for doping: 450 or 500 °C. Glass substrates were used for deposition. All molybdenum-containing films were matte gray to black in color. Chromium-only films were uniform and mirrored in their visual appearance. All films were solid and fully adherent to the glass substrates and were not dusty or mobile in any way.

The elemental compositions of the films produced were analyzed by energy dispersive X-ray (EDX) spectroscopy. Films of MoS₂ grown at both temperatures from **MoL₄** were analyzed as MoS₂ (Theory: Mo 33 mol %, S 66 mol %. Found: 450 °C, Mo 31 mol %, S 69 mol %; 500 °C, Mo 36 mol %, S 63 mol %), and those grown from **CrL₃** were analyzed as CrS (Theory: Cr 50 mol %, S 50 mol %. Found: 450 °C, Cr 55 mol %, S 45 mol %; 500 °C, Cr 55 mol %, S 45 mol %). Using EDX spectroscopy, it was also possible to confirm that for dual source precursor experiments, doping of chromium into the MoS₂ structure had been successful (Figure 1). The amount of chromium found in the films experimentally by EDX spectroscopy was always less than the theoretical amount of chromium in the precursor mixture, though a linear trend is clear for both deposition temperatures ($R^2_{450\text{ }^\circ\text{C}} = 0.8799$,

$R^2_{500\text{ }^\circ\text{C}} = 0.9591$). There is little difference in the amount of chromium in films deposited at either 450 °C ($y = 0.40x \pm 0.10x$) or 500 °C ($y = 0.36x \pm 0.08x$) for the same precursor ratios. Hence, we conclude tentatively that the availability of precursors is diffusion-limited at both temperatures, and thus, the effect of temperature on the elemental composition in the temperature range studied is minimal. Secondary electron scanning electron microscopy (SEM) imaging of the thin films revealed their surface morphology. MoS₂ films with no dopant, produced by the method of O'Brien and co-workers,¹ exhibited leaf-like lamellar morphologies. Films of the same material with chromium doped into them, however, displayed an increasing propensity toward granular morphology (Figure 2).

Changes in the Raman spectra upon doping were also observed. Raman spectra of the purely MoS₂ displayed its strongest Raman band at a shift of 408 cm⁻¹ (D_{6h} out-of-plane phonon mode of A_{1g} symmetry involving S atoms^{41,42}). Upon increasing the amount of chromium in the films, the intensity of the LA(M) longitudinal acoustic mode⁴² at 227 cm⁻¹ was enhanced. By taking the ratio of the peak intensity of the LA(M) band to the A_{1g} band, and plotting these values versus the amount of chromium determined experimentally by EDX spectroscopy for each film, we were able to construct a curve for each deposition temperature (Figure 3). For both

temperatures, as more chromium is doped into the MoS₂, the value of (I_{227}/I_{408}) becomes closer to unity and reaches a plateau as it approaches 15–20 mol % Cr for films generated at both temperatures. Hence, Raman spectroscopy is an expedient technique in this case compared to EDX spectroscopy, providing a useful way to rapidly quantify the amount of Cr dopant in such films in the 0–15% region. Additionally, Raman spectroscopy could prove useful for the quantification of other metal dopants in MoS₂ in future studies.

Films were analyzed using powder X-ray diffraction (pXRD). Molybdenum-containing films showed strong preferred orientation in the (002) plane, that is, arrangement of the hexagonal planes of MoS₂ parallel to the substrate surface (x, y plane). The peak position of the (002) reflection was observed to shift to higher 2θ values (and thus lower d -spacing) as the amount of chromium doped into the structure increased (Figure 4). Plots of the calculated d -spacing versus the amount

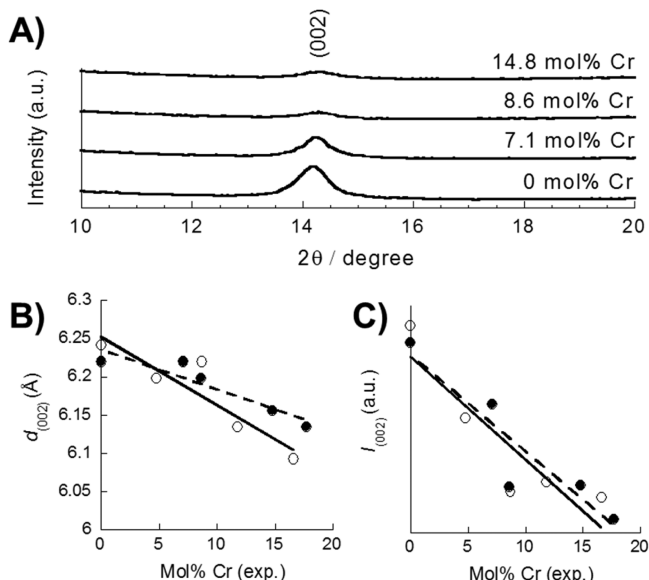


Figure 4. Analysis of chromium-doped MoS₂ thin films by powder X-ray diffraction. (A) Powder X-ray diffraction patterns for MoS₂ thin films containing varying amounts of chromium deposited at 450 °C, deliberately y -offset for clarity. (B) Changes in d -spacing for the (002) plane vs chromium dopant found experimentally using EDX spectroscopy for deposition at 450 °C (●) and 500 °C (○). (C) Changes in the intensity of the (002) reflection vs chromium dopant found experimentally using EDX spectroscopy for deposition at 450 °C (● and linear fit - - -) and 500 °C (○ and linear fit —).

of chromium found experimentally in the films show an almost linear dependence. This suggests that the doping of chromium into the MoS₂ structure tends to contract the structure in the z -direction, pulling the layers of MoS₂ together. It was also noted that the (002) peak intensity diminishes and broadens as more chromium is doped into the MoS₂ (Figure 4 and Supporting Information), suggesting that the particle crystallite size diminishes with increased doping. The latter is likely and indeed observed by SEM (vide supra); the incorporation of Ni as a dopant into MoS₂ has been shown by X-ray extended absorption fine structure (EXAFS) to introduce NiO_x at the edge sites of MoS₂, limiting the crystal size attainable within films due to termination of growth of nucleating MoS₂.⁴³ pXRD analysis of the CrS films did not show any lattice reflections,

and these are therefore likely to be amorphous (Supporting Information).

Films were further investigated using atomic force microscopy (AFM). AFM images produced from the height profile of films demonstrate a gradual transition from lamellar to a more granulated morphology as the amount of Cr dopant in the films increases (Figure 5), in agreement with the observations made by SEM and the vanishing (002) peak in the pXRD patterns. There is perhaps evidence of some nanostructured features, especially for films with higher chromium content. CrS films are composed of granulated features.

The nanomechanical properties of the films were also elucidated using AFM. The results of the measurement of the arbitrary elastic modulus (E_{arb} , relative to the MoS₂ sample produced at each temperature, where $E_{\text{arb}, \text{MoS}2} = 1.0$) calculated using a 10-point mean from automated real-time analysis of force curves using the Derjaguin–Muller–Toporov (DMT) model of contact mechanics⁴⁴ with windows of interrogation of 1 μm^2 for each film are presented in Table 1. It can be seen that for Cr-doped films at both deposition temperatures, the maximum modulus of elasticity is experienced for films with 5–10 mol % Cr dopant. This is perhaps consistent with findings reported previously, where levels of 5–15% Cr produced superior hardness or endurance compared to the parent compound, MoS₂.^{27,28} The material with the largest relative elasticity compared to MoS₂ is CrS produced at 500 °C.

In order to further explore the nature of the doping, and specifically the nanoscale distribution of the Cr dopant within the MoS₂ sheets, two films (0% Cr, 450 °C and 7.1% Cr, 450 °C) were immersed in N-methyl-2-pyrrolidone (NMP) and ultrasonically exfoliated.^{9,45} The exfoliated samples produced were then analyzed by transmission electron microscopy (TEM), high-angle annular dark-field scanning transmission electron microscopy (HAADF STEM) imaging, and EDX spectrum imaging (Figures 6 and 7). The undoped exfoliated MoS₂ flakes appear to consist of highly crystalline nanosheets with typical diameters greater than 300 nm. Deconvoluted elemental maps extracted from the EDX spectrum images reveal that, as expected, the Mo and S are distributed evenly throughout the sheets. Analysis of both the individual spectra and the summed spectrum images reveals that no Cr is present in the sample. TEM and HAADF images of the 7.1% Cr-doped MoS₂ sample reveal similar sized flakes to those found in the undoped sample. However, high-resolution imaging reveals that these flakes often consist of bundles of small randomly oriented nanosheets, giving credence to the argument suggested by XRD that chromium doping reduces crystallite size, perhaps through the inhibition of nanosheet growth by edge-site termination.

Three possible models can be suggested for the chromium incorporation. The first is a substitutional alloy in which chromium centers replace molybdenum centers.⁴⁶ The second, with chromium in interstitial sites between the sulfur layers. This second postulate is known for metal ions such as lithium and is often exploited for exfoliation purposes.⁴⁷ The third is that chromium centers occupy edge sites at the termini of MoS₂ planes, the so-called S-edge ($\bar{1}\bar{1}0$), parallel to the basal plane. This mode of incorporation is well-known for transition metal dopants such as cobalt, and indeed, it is of great interest for modification of hydrogen-evolution properties in both MoS₂ and WS₂, where the active catalytic sites occur at the edges of the hexagonal lamellae.⁴⁸ Cobalt and nickel are known to cause major morphological changes to the structure of MoS₂ from basal plane truncations caused by binding at edge sites;^{43,49} this

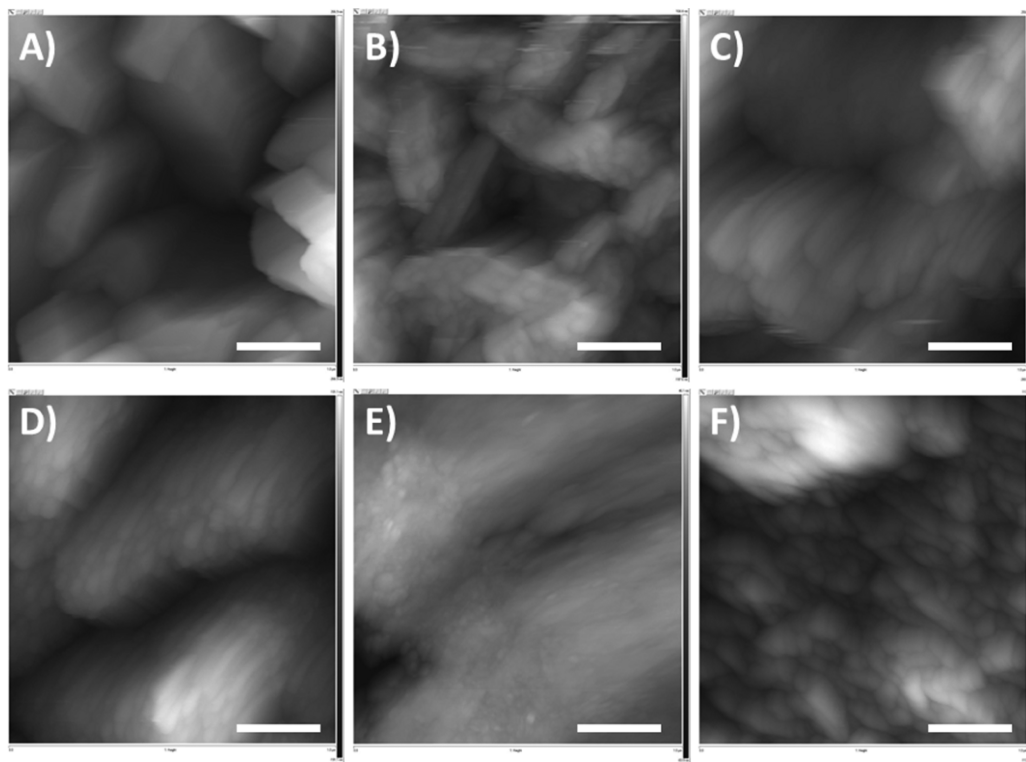


Figure 5. Height profile images produced from atomic force microscopy of thin films grown at 450 °C. (A) MoS₂, (B) 7.1 mol % Cr, (C) 8.6 mol % Cr, (D) 14.8 mol % Cr, (E) 17.7 mol % Cr, (F) CrS. Scale bars = 250 nm.

Table 1. Elemental Composition (EDX Spectroscopy), Deposition Temperature, and Arbitrary Elastic Modulus (E_{arb}) Measured for Thin Films Using AFM, Relative to MoS₂ Films

film composition by EDXS	deposition temperature (°C)	arbitrary elastic modulus (E_{arb})
MoS ₂ – 31% Mo 69% S	450	1.0
MoS ₂ + 7.1% Cr	450	1.4
MoS ₂ + 8.6% Cr	450	1.0
MoS ₂ + 14.8% Cr	450	0.5
MoS ₂ + 17.7% Cr	450	0.4
CrS – 55% Cr 45% S	450	1.2
MoS ₂ – 36% Mo 63% S	500	1.0
MoS ₂ + 4.8% Cr	500	2.0
MoS ₂ + 8.7% Cr	500	0.8
MoS ₂ + 11.8% Cr	500	1.5
MoS ₂ + 16.6% Cr	500	N/A ^a
CrS – 55% Cr 45% S	500	2.3

^aCould not be measured due to roughness of film.

mode of binding could indeed be apparent in Cr-doped MoS₂ from the SEM, pXRD, AFM, and HAADF STEM results considered here, particularly if truncation leads to the formation of smaller sheets. EDX spectrum imaging of flakes reveals that the chromium is distributed rather evenly throughout the MoS₂ layers at 10 nm spatial resolution, but these results do not rule out the presence of Cr at edge sites. It must therefore be concluded from the results of the various analyses that a number of dopant modes are possible, and the exact nature of the chromium incorporation within the films still remains to be elucidated. Toward this end, further experiments are planned using high-resolution scanning transmission electron micro-

copy of the Cr-doped MoS₂ flakes at atomic-level resolution,⁵⁰ to attempt to directly elucidate the location of the dopant ions.

CONCLUSIONS

We have successfully grown Cr-doped MoS₂ films on glass substrates by AACVD using single-molecule precursors in tandem. We have also been able to grow CrS films from a chromium dithiocarbamate precursor. EDX spectroscopy confirmed the presence and composition of chromium in the films and SEM demonstrated changes in morphology for films incorporating increasing amounts of chromium. The Cr-doping caused measurable perturbations in the Raman spectra of MoS₂ films, allowing ratiometric determination of the amount of dopant. Changes in both the intensity and peak position of the (002) planes upon increasing amount of Cr dopant were observed in the pXRD patterns of thin films suggesting that the Cr dopant produced small changes in the crystallite morphology. CrS films produced appeared to be amorphous according to their pXRD pattern. AFM was used to confirm changes in morphology observed by SEM as well as to investigate the nanomechanical properties of the films. Doped films with 5–10 mol % Cr were found to exhibit relatively larger moduli of elasticity compared to films composed of MoS₂. It is reasonable therefore to suggest that these doped films will have potential to be more persistent compared to the parent compound and thus may be relatively better antiwear materials for automotive engines.

Additionally, the ability to produce metal-doped MoS₂ in a facile manner by AACVD, followed by liquid-phase exfoliation in NMP to give few-layer doped nanosheets (n.b. both potentially scalable processes; e.g., AACVD has recently been used in a similar system to ours to coat TiO₂ and float glass substrates of 40 cm² area with CH₃CH₂NH₃PbI₃, an

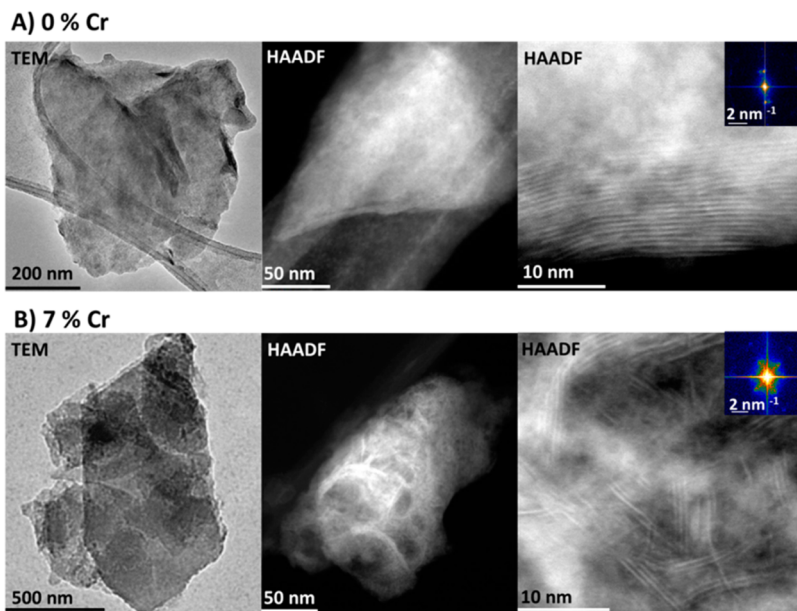


Figure 6. TEM imaging and HAADF STEM imaging of (A) undoped ($0\text{ mol } \% \text{Cr}$, $450\text{ }^\circ\text{C}$) and (B) doped ($7.1\text{ mol } \% \text{Cr}$, $450\text{ }^\circ\text{C}$) MoS_2 nanosheets, respectively. Bright-field TEM images (left-hand images) and HAADF STEM images (center and right images) show the exfoliated flakes are typically $>300\text{ nm}$ in diameter. High-resolution HAADF STEM images (right-hand images) of the undoped and doped samples, revealing atomic planes within the nanosheets (inset are Fourier transforms showing the different lattice orientations). The doped sample contains bundles of small randomly orientated flakes (although larger nanosheets with more uniform crystal structure are also found), whereas the undoped sample only shows larger highly crystalline sheets.

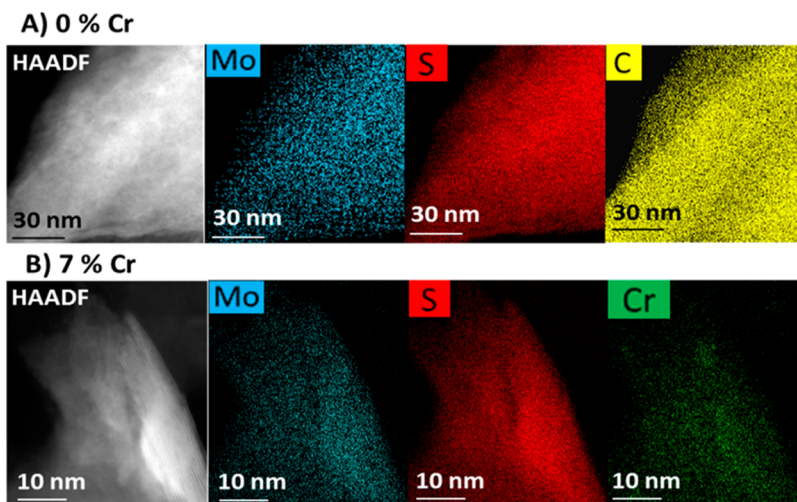


Figure 7. HAADF STEM and EDX spectrum imaging of (A) undoped ($0\text{ mol } \% \text{Cr}$, $450\text{ }^\circ\text{C}$) and (B) doped ($7.1\text{ mol } \% \text{Cr}$, $450\text{ }^\circ\text{C}$) MoS_2 nanosheets, respectively. Deconvoluted elemental maps extracted from EDX spectrum images show that in both cases Mo and S are distributed uniformly throughout the flake at a spatial resolution approaching 10 nm . Carbon signal in (A) is from the amorphous carbon support film. For the doped sample in (B) the nanoscale distribution of Cr is found to be fairly uniform while for the undoped sample no Cr signal is detected.

inorganic–organic halide perovskite important in photovoltaics,^{37,51} and atmospheric pressure CVD has been used to deposit MoS_2 itself over areas $>1000\text{ mm}^2$ in size⁵²) could be useful in applications such as inkjet printing⁵³ (as has been demonstrated for MoS_2 itself⁵²) of metal-doped MoS_2 nanosheets to allow new device applications by perturbation of the electronic properties of MoS_2 , which will be especially stimulating for the development of all-printed hybrid two-dimensional devices alongside materials such as graphene, hexagonal boron nitride and other metal chalcogenides,³³ and phosphorene³⁸ which could potentially have new and exciting electronic properties.

■ ASSOCIATED CONTENT

S Supporting Information

Powder X-ray diffraction patterns of CrS thin films on glass substrates; crystallography data and single crystal X-ray structure of CrL_3 ; thermogravimetric analysis curve for CrL_3 ; full powder X-ray diffraction patterns of MoS_2 and Cr-doped MoS_2 films grown at $450\text{ }^\circ\text{C}$ by AACVD. This material is available free of charge via the Internet at <http://pubs.acs.org>.

AUTHOR INFORMATION

Corresponding Author

*Email: Paul.O'Brien@manchester.ac.uk. Tel: +44 (0) 161 275 4653. http://www.icam-online.org.

Notes

The authors declare no competing financial interest.

ACKNOWLEDGMENTS

D.J.L. and A.A.T. are funded by ICAM. S.J.H., A.R., and E.A.L thank the U.S.A. Defense Threat Reduction Agency (grant no. HDTRA1-12-1-0013) as well as NoWNano CDT (EPSRC grant no. EP/G03737X/1) for funding support. The authors also wish to acknowledge funding support from H.M. Government (U.K.) for the FEI Titan G2 80-200 S/TEM associated with research capability of the Nuclear Advanced Manufacturing Research Centre. Some of the equipment used in this study were provided by the Engineering and Physical Sciences Research Council (*Core Capability in Chemistry*, EPSRC grant number EP/K039547/1). We would like to thank Dr. Caitlin Rice (University of Manchester) for useful discussion regarding MoS₂ Raman spectral features and Dr. M. Azad Malik (University of Manchester) for useful discussions.

REFERENCES

- (1) Adeogun, A.; Afzaal, M.; O'Brien, P. *Chem. Vap. Deposition* **2006**, *12*, 597–599.
- (2) Chhowalla, M.; Amarantunga, G. A. J. *Nature* **2000**, *407*, 164–167.
- (3) Rosentsveig, R.; Gorodnev, A.; Feuerstein, N.; Friedman, H.; Zak, A.; Fleischer, N.; Tannous, J.; Dassenoy, F.; Tenne, R. *Tribol. Lett.* **2009**, *36*, 175–182.
- (4) Rosentsveig, R.; Margolin, A.; Gorodnev, A.; Popovitz-Biro, R.; Feldman, Y.; Rapoport, L.; Novema, Y.; Naveh, G.; Tenne, R. *J. Mater. Chem.* **2009**, *19*, 4368–4374.
- (5) Tenne, R.; Redlich, M. *Chem. Soc. Rev.* **2010**, *39*, 1423–1434.
- (6) Novoselov, K. S.; Jiang, D.; Schedin, F.; Booth, T. J.; Khotkevich, V. V.; Morozov, S. V.; Geim, A. K. *Proc. Natl. Acad. Sci. U.S.A.* **2005**, *102*, 10451–10453.
- (7) Matte, H. S. S. R.; Gomathi, A.; Manna, A. K.; Late, D. J.; Datta, R.; Pati, S. K.; Rao, C. N. R. *Angew. Chem., Int. Ed.* **2010**, *49*, 4059–4062.
- (8) Zhang, X.; Xie, Y. *Chem. Soc. Rev.* **2013**, *42*, 8187–8199.
- (9) Coleman, J. N.; Lotya, M.; O'Neill, A.; Bergin, S. D.; King, P. J.; Khan, U.; Young, K.; Gaucher, A.; De, S.; Smith, R. J.; Shvets, I. V.; Arora, S. K.; Stanton, G.; Kim, H.-Y.; Lee, K.; Kim, G. T.; Duesberg, G. S.; Hallam, T.; Boland, J. J.; Wang, J. J.; Donegan, J. F.; Grunlan, J. C.; Moriarty, G.; Shmeliov, A.; Nicholls, R. J.; Perkins, J. M.; Grieveson, E. M.; Theuwissen, K.; McComb, D. W.; Nellist, P. D.; Nicolosi, V. *Science* **2011**, *331*, 568–571.
- (10) Miro, P.; Audiffred, M.; Heine, T. *Chem. Soc. Rev.* **2014**, *43*, 6537–6554.
- (11) Zhou, W.; Zou, X.; Najmaei, S.; Liu, Z.; Shi, Y.; Kong, J.; Lou, J.; Ajayan, P. M.; Yakobson, B. I.; Idrobo, J.-C. *Nano Lett.* **2013**, *13*, 2615–2622.
- (12) Daage, M.; Chianelli, R. R. *J. Catal.* **1994**, *149*, 414–427.
- (13) Hinnemann, B.; Moses, P. G.; Bonde, J.; Jorgensen, K. P.; Nielsen, J. H.; Horch, S.; Chorkendorff, I. *Science* **2007**, *317*, 100–102.
- (14) Jaramillo, T. F.; Jorgensen, K. P.; Bonde, J.; Nielsen, J. H.; Horch, S.; Chorkendorff, I. *Science* **2007**, *317*, 100–102.
- (15) Spikes, H. *Tribol. Lett.* **2004**, *17*, 469–489.
- (16) Scharf, T. W.; Prasad, S. V. *J. Mater. Sci.* **2013**, *48*, 511–531.
- (17) Dickinson, R. G.; Pauling, L. *J. Am. Chem. Soc.* **1923**, *45*, 1466–1471.
- (18) Winer, W. O. *Wear* **1967**, *10*, 422–452.
- (19) Amelinckx, A. *Discuss. Farad. Soc.* **1964**, *38*, 7–26.
- (20) Martin, J. M.; Donnet, C.; Lemogne, T.; Epicier, T. *Phys. Rev. B* **1993**, *48*, 10583–10586.
- (21) Petrescu, M. I. *Acta Cryst. B* **2012**, *B68*, 501–510.
- (22) Shtanskii, D. V.; Kulich, S. A.; Levashov, E. A.; Moore, J. J. *Phys. Solid State* **2003**, *45*, 1177–1184.
- (23) Lazell, M.; O'Brien, P.; Otway, D. J.; Park, J. H. *Dalton Trans.* **2000**, *4479*–4486.
- (24) Marchand, P.; Hassan, I. A.; Parkin, I. P.; Carmalt, C. J. *Dalton Trans.* **2013**, *42*, 9406–9422.
- (25) Malik, M. A.; Afzaal, M.; O'Brien, P. *Chem. Rev.* **2010**, *110*, 4417–4446.
- (26) McCain, M. N.; He, B.; Sanati, J.; Wang, Q. J.; Marks, T. J. *Chem. Mater.* **2008**, *20*, 5438–5443.
- (27) Stupp, B. C. *Thin Solid Films* **1981**, *84*, 257–266.
- (28) Ding, X.-z.; Zeng, X. T.; He, X. Y.; Chen, Z. *Surf. Coat. Technol.* **2010**, *205*, 224–231.
- (29) Kao, W. H.; Su, Y. L. *Mater. Sci. Eng., A* **2004**, *368*, 239–248.
- (30) Fenker, M.; Balzer, M.; Kappl, H.; Savan, A. *Surf. Coat. Technol.* **2006**, *201*, 4099–4104.
- (31) Simmonds, M. C.; Savan, A.; Pfleiderer, E.; Van Swygenhoven, H. *Surf. Coat. Technol.* **2000**, *126*, 15–24.
- (32) Finn, D. J.; Lotya, M.; Cunningham, G.; Smith, R. J.; McCloskey, D.; Donegan, J. F.; Coleman, J. N. *J. Mater. Chem. C* **2014**, *2*, 925–932.
- (33) Withers, F.; Yang, H.; Britnell, L.; Rooney, A. P.; Lewis, E.; Felten, A.; Woods, C. R.; Sanchez Romaguera, V.; Georgiou, T.; Eckmann, A.; Kim, Y. J.; Yeates, S. G.; Haigh, S. J.; Geim, A. K.; Novoselov, K. S.; Casiraghi, C. *Nano Lett.* **2014**, *14*, 3987–3992.
- (34) Sheldrick, G. M. *Acta Crystallogr., Sect. A* **2008**, *64*, 112–122.
- (35) Decoster, M.; Conan, F.; Guerchais, J. E.; Lemest, Y.; Pala, J. S.; Jeffery, J. C.; Faulques, E.; Leblanc, A.; Molinie, P. *Polyhedron* **1995**, *14*, 1741–1750.
- (36) Ramasamy, K.; Kuznetsov, V. L.; Gopal, K.; Malik, M. A.; Raftery, J.; Edwards, P. P.; O'Brien, P. *Chem. Mater.* **2013**, *25*, 266–276.
- (37) Lewis, D. J.; O'Brien, P. *Chem. Commun.* **2014**, *50*, 6319–6321.
- (38) Brent, J. R.; Savjani, N.; Lewis, E. A.; Haigh, S. J.; Lewis, D. J.; O'Brien, P. *Chem. Commun.* **2014**, *50*, 13338–13341.
- (39) Golding, R. M.; Healy, P. C.; Colombera, P.; W. A. H. *Aust. J. Chem.* **1974**, *27*, 2089–2097.
- (40) Raston, C. L.; White, A. H. *Aust. J. Chem.* **1977**, *30*, 2091–2094.
- (41) Molina-Sanchez, A.; Wirtz, I. *Phys. Rev. B* **2011**, *84*, 155413.
- (42) Li, H.; Zhang, Q.; Yap, C. C. R.; Tay, B. K.; Edwin, T. H. T.; Olivier, A.; Baillargeat, D. *Adv. Funct. Mater.* **2012**, *22*, 1385–1390.
- (43) Lince, J. R.; Hilton, M. R.; Bommannavar, A. S. *J. Mater. Res.* **1995**, *10*, 2091–2105.
- (44) Wang, D.; Russell, T. P.; Nishi, T.; Nakajima, K. *ACS Macro Lett.* **2013**, *2*, 757–760.
- (45) Savjani, N.; Lewis, E. A.; Patrick, R. A. D.; Haigh, S. J.; O'Brien, P. *RSC Adv.* **2014**, *4*, 35609–35613.
- (46) Yue, Q.; Chang, S.; Qin, S.; Li, J. *Phys. Lett. A* **2013**, *377*, 1362–1367.
- (47) Eda, G.; Yamaguchi, H.; Voiry, D.; Fujita, T.; Chen, M.; Chhowalla, M. *Nano Lett.* **2011**, *11*, 5111–5116.
- (48) Bonde, J.; Moses, P. G.; Jaramillo, T. F.; Norskov, J. K.; Chorkendorff, I. *Faraday Discuss.* **2009**, *140*, 219–231.
- (49) Brorson, M.; Carlsson, A.; Topsøe, H. *Catal. Today* **2007**, *123*, 31–36.
- (50) Hansen, L. P.; Ramasse, Q. M.; Kisielowski, C.; Brorson, M.; Johnson, E.; Topsøe, H.; Helveg, S. *Angew. Chem., Int. Ed.* **2011**, *50*, 10153–10156.
- (51) Bhachu, D. S.; Scanlon, D. O.; Saban, E. J.; Bronstein, H.; Parkin, I. P.; Carmalt, C. J.; Palgrave, R. G. *J. Mater. Chem. A* **2015**, DOI: 10.1039/c4ta05522e.
- (52) Huang, C.-C.; Al-Saab, F.; Wang, Y.; Ou, J.-Y.; W. J. C.; Wang, S.; Gholipour, B.; Simpson, R. E.; Hewak, D. W. *Nanoscale* **2014**, *6*, 12792–12797.
- (53) Derby, B. *Annu. Rev. Mater. Res.* **2010**, *40*, 395–414.